The Journal of Chemical Physics

An efficient hybrid scheme for time dependent density functional theory

Cite as: J. Chem. Phys. **152**, 184104 (2020); https://doi.org/10.1063/5.0005954
Submitted: 26 February 2020 . Accepted: 16 April 2020 . Published Online: 12 May 2020

Marco Medves, Luca Sementa, Daniele Toffoli, Giovanna Fronzoni, Alessandro Fortunelli, and Mauro Stener

AIP Publishing

The Journal of Chemical Physics ARTICLE scitation.org/journal/jcp

An efficient hybrid scheme for time dependent density functional theory

Cite as: J. Chem. Phys. 152, 184104 (2020); doi: 10.1063/5.0005954
Submitted: 26 February 2020 • Accepted: 16 April 2020 •
Published Online: 12 May 2020

Marco Medves,[1] Luca Sementa,[2] Daniele Toffoli,[1] Giovanna Fronzoni,[1] Alessandro Fortunelli,[2,a)] and Mauro Stener[1,b)]

AFFILIATIONS

[1] Dipartimento di Scienze Chimiche e Farmaceutiche, Università di Trieste, Via Giorgieri 1, 34127 Trieste, Italy
[2] CNR-ICCOM & IPCF, Consiglio Nazionale delle Ricerche, Via Giuseppe Moruzzi 1, 56124 Pisa, Italy

[a)] **E-mail:** alessandro.fortunelli@cnr.it
[b)] **Author to whom correspondence should be addressed:** stener@units.it

ABSTRACT

A hybrid approach able to perform Time Dependent Density Functional Theory (TDDFT) simulations with the same accuracy as that of hybrid exchange-correlation (xc-) functionals but at a fraction of the computational cost is developed, implemented, and validated. The scheme, which we name Hybrid Diagonal Approximation (HDA), consists in employing in the response function a hybrid xc-functional (containing a fraction of the non-local Hartree–Fock exchange) only for the diagonal elements of the omega matrix, while the adiabatic local density approximation is employed for the off-diagonal terms. HDA is especially (but not exclusively) advantageous when using Slater type orbital basis sets and allows one to employ them in a uniquely efficient way, as we demonstrate here by implementing HDA in a local version of the Amsterdam Density Functional code. The new protocol is tested on NH_3, C_6H_6, and the $[Au_{25}(SCH_3)_{18}]^-$ cluster as prototypical cases ranging from small molecules to ligand-protected metal clusters, finding excellent agreement with respect to both full kernel TDDFT simulations and experimental data. Additionally, a specific comparison test between full kernel and HDA is considered at the Casida level on seven other molecular species, which further confirm the accuracy of the approach for all investigated systems. For the $[Au_{25}(SCH_3)_{18}]^-$ cluster, a speedup by a factor of seven is obtained with respect to the full kernel. The HDA, therefore, promises to provide a quantitative description of the optical properties of medium-sized systems (nanoclusters) at an affordable cost, thanks to its computational efficiency, especially in combination with a complex polarization algorithm version of TDDFT.

I. INTRODUCTION

Chiro-optical absorption spectra represent one of the most direct, routine, and cheap experimental probes in chemistry, providing important information on the electronic structure of the system under study. For complex systems, however, a reliable assignment of the observed spectral features, leading to their rationalization and, eventually, design, is not straightforward. In this context, theory and computational simulations play an increasingly crucial role in arriving at an in-depth understanding of experimental observations.[1] The development and implementation of efficient computational schemes for the calculation of molecular photoabsorption spectra that can enable predictive simulations of complex systems is, thus, a very active area of current research.[1] Time Dependent Density Functional Theory (TDDFT) has gained a leader role in this race, due to its optimal compromise between accuracy and computational economy. The most popular TDDFT implementation in quantum chemistry has been proposed by Casida,[2] which corresponds to a density-matrix approach according to the classification by Görling *et al.*[3] and consists in setting up and solving an eigenvalue problem over a basis of single-particle excitations. In addition to the Casida one, other TDDFT formulations have been developed and successfully implemented, which are briefly summarized as follows. One is based on an explicit time-propagation technique. This scheme was introduced in the pioneering work of Yabana and Bertsch[4] and is typically implemented over real space grids, like in the OCTOPUS code.[5] Another possibility is based on a super-operator formulation of TDDFT and has been implemented employing a Lanczos method and plane wave basis set.[6] The third, a more recent scheme, has been introduced by Grimme, and it consists in a simplified

Tamm–Dancoff Approximation (TDA)[7] and TDDFT.[8] A linear-scaling TDDFT has been developed by Zuehlsdorff *et al.*[9] An efficient method for large systems is the TDDFT time-propagation by Malola *et al.*[10] Recently, Noda *et al.* have developed a massively parallel implementation of TDDFT based on real time and real space,[11] which allowed them to study clusters containing up to 1414 gold atoms.[12] Finally, a complex polarizability algorithm for TDDFT[13–15] (called polTDDFT in the following) is particularly suitable for application to very large systems and will also be employed in the present work.[16]

These methods, especially the more recent ones, have achieved a high level of computational efficiency, allowing, nowadays, the treatment of molecules containing several hundreds of atoms at the TDDFT level.[12,16] Accuracy is, however, a more complicated issue at both DFT and TDDFT levels since it depends crucially on the choice of the exchange-correlation (xc-) functional employed to derive DFT Kohn–Sham (KS) orbitals and energies and in the response kernel of TDDFT. Although the search for increasingly more accurate xc-functionals and kernels is still active and new proposals appear continuously in the literature,[17,18] at the moment, the most accurate and popular choices correspond to hybrid xc-functionals for both DFT and TDDFT kernels, i.e., functionals containing a variable fraction of the exact [Hartree–Fock (HF)] non-local exchange. Among hybrid xc-functionals, B3LYP[19,20] is the most widely utilized one. B3LYP has the advantage of being rather versatile, that is, of performing reasonably well for both ground state (geometry optimization, bonding energy, and vibrational frequencies) and excited state (photoabsorption spectra) properties. Moreover, B3LYP has recently proven to be able to successfully describe vibronic effects in core electron excitations (NEXAFS) at the TDDFT level[21] and core electron ionization (XPS) at the DFT level within the ΔSCF scheme.[22] Some limitations have, however, shown up in special instances, such as, for example, the absence of Rydberg states due to the lack of a correct asymptotic Coulombic behavior or the prediction of core-excited spectra shifted by several eV with respect to the experiment. Both deficiencies can be solved: the former, by adding Long-range Correction (LC),[23] and the latter, by adding Short-range Correction (SC)[24] to B3LYP. In this work, we will, therefore, implement and test our approach using the B3LYP functional although the scheme we propose here is quite general and can hold for any hybrid functionals.

It should be recalled that the use of hybrid functionals may present severe numerical issues connected with the HF non-local exchange, whose evaluation over basis sets involves matrix elements that can be treated efficiently when basis sets of Gaussian Type Orbitals (GTOs) are employed, but becomes problematic with other basis sets, such as Slater Type Orbitals (STOs) or Plane Waves (PWs). It should be observed that when using STO basis sets and hybrid xc-functionals, the SCF procedure becomes less efficient but is still computationally affordable even for large systems, whereas the TDDFT problem becomes soon intractable due to the extremely heavy computational cost of the HF non-local part of the kernel.

To solve these issues and arrive at an operational and efficient TDDFT approach employing hybrid xc-functionals, in the present work, we propose, develop, and validate an approximate treatment of the TDDFT kernel, which we call Hybrid Diagonal Approximation (HDA), and justify it by simple theoretical arguments. The HDA is based on utilizing the hybrid exchange only for the diagonal terms in the response equations: this allows one to limit the computational cost of the TDDFT simulation while keeping basically the same accuracy as in the full TDDFT scheme using hybrid xc-functionals, as we will demonstrate hereafter. We implement our HDA approach both in the conventional Casida TDDFT scheme and in the more recent polTDDFT complex polarizability algorithm,[13] within a local version of the Amsterdam Density Functional (ADF) package, which will be distributed in a forthcoming release. Although the present work focuses on the implementation of HDA using STO basis sets, the fundamental idea behind the HDA approach is completely general and can be profitably extended to other basis sets as well, such as plane waves.

The article is organized as follows: we first provide a theoretical justification of the HDA. We then describe its implementation for both Casida and polTDDFT complex polarizability algorithms. Third, we validate and benchmark the method by comparing its results with respect to a standard Casida approach employing B3LYP in both DFT and in the TDDFT kernel, as well as with accurate experimental data for small systems (NH_3 and C_6H_6). We also validate our approach on a larger system, a medium-sized metal cluster $[Au_{25}(SR)_{18}]^-$, for which both the x-ray crystal structure and the experimental optical absorption spectrum are available, in order to demonstrate the computational efficiency and economy of the HDA. Finally, we test the HDA with respect to the full kernel at the Casida level for seven other systems, in order to corroborate the general validity of the suggested approximation and provide information regarding the errors introduced by this scheme.

II. THEORETICAL METHOD AND IMPLEMENTATION

A. Casida TDDFT formulation

The standard (and most widely employed) TDDFT formulation in quantum chemistry consists in expanding the molecular Kohn–Sham (KS) orbitals as a linear combination of atomic functions and recast the TDDFT equations in terms of a diagonalization of a matrix omega (Ω) according to the density-matrix formulation of Casida.[2] In practice, the KS equations are first solved,

$$H_{KS}\varphi_i = \varepsilon_i\varphi_i\,. \tag{1}$$

Then, the Ω matrix is diagonalized,

$$\Omega\mathbf{F}_I = \omega_I^2\mathbf{F}_I\,, \tag{2}$$

where the matrix elements of the Ω matrix can be calculated from the solution of KS equation (1):

$$\Omega_{ia,jb} = \delta_{ij}\delta_{ab}(\varepsilon_a - \varepsilon_i)^2 + 2\sqrt{\varepsilon_a - \varepsilon_i}K_{ia,jb}\sqrt{\varepsilon_b - \varepsilon_j}\,, \tag{3}$$

and in expression (3), the coupling matrix $K_{ia,jb}$ is defined as

$$K_{ia,jb} = \langle aj|\,ib\rangle + \langle aj|f_{\sigma\tau}^{XC}|ib\rangle. \tag{4}$$

In Eq. (4), $f_{\sigma\tau}^{XC}$ is the xc-kernel, with σ and τ being spin variables. The Casida problem consists in finding eigenvalues and eigenvectors of Ω, Eq. (2). The eigenvalues of (2) correspond to the squared excitation energies, while from the eigenvectors, the intensities (absolute oscillator strengths) can be extracted.[2] It is worth noting that the Ω matrix elements span the first-order density matrix,

which corresponds to all the products between occupied and virtual KS orbitals, so that the dimension of the Ω matrix is Nocc × Nvirt and can be quite large (≈10^5) for a cluster containing more than 100 metal atoms. The Casida approach is efficiently implemented in many quantum chemistry codes, such as, for example, ADF code,[25–27] which takes advantages of the molecular symmetry (employing the Wigner–Eckart theorem for the TDDFT part), of the Davidson diagonalization algorithm, of efficient fitting techniques of the first-order density through the use of auxiliary basis functions to improve matrix-vector multiplication within the Davidson algorithm, and finally of the parallelization of the code which can exploit modern supercomputer architectures. Although the formalism is quite general, issues can arise when hybrid xc-functionals and xc-kernels are chosen. When GTO are utilized, hybrid functionals and kernels can be implemented without hampering numerical efficiency, due to the availability of analytic formulas for non-local exchange integrals (although for large molecules, density fitting techniques[28,29] must be used, which can be problematic with large basis sets). On the contrary, many problems arise when using non-GTO basis sets, such as STO or PW. When STO are employed, non-local exchange integrals can be calculated in practice by means of density fitting techniques,[28,29] which allow one to approximate a product of STO centered on different atoms as a linear combination of auxiliary functions, employed to fit the electron density. This allows one to solve the DFT KS equations with a reasonable effort also for large systems, but in TDDFT, the non-local kernel becomes soon impracticable. For example, for a moderate-size metal cluster such as $Au_{25}(SR)_{18}$, the TDDFT part calculated with hybrid B3LYP kernel *needs* 60 *times more central processing unit* (*CPU*)*-time* than a conventional generalized gradient approximation (GGA), i.e., non-hybrid calculation. It would then be appealing to reduce the computational effort of the hybrid xc-kernel without giving up to the high accuracy afforded by the use of hybrid xc-functionals for the description of the electronic structure of the systems under study.

A first possibility would be to employ the hybrid functional only for the DFT KS part and use the Adiabatic Local Density Approximation (ALDA)[30] for the TDDFT kernel. However, the presence of the non-local HF exchange in the KS equations causes a relevant shift (up to several eV) of the virtual orbital eigenvalues to higher energies rendering the calculated spectrum inaccurate. It is worth noting at this point that when a hybrid kernel is used, this effect is compensated by a shift in the opposite direction of the diagonal elements of the matrix, caused by the non-local HF exchange of the xc-kernel. This is best seen by casting the TDDFT equations in the Random Phase Approximation (RPA) structure,

$$\begin{pmatrix} A & B \\ B^* & A^* \end{pmatrix}\begin{pmatrix} X \\ Y \end{pmatrix} = \omega \begin{pmatrix} 1 & 0 \\ 0 & -1 \end{pmatrix}\begin{pmatrix} X \\ Y \end{pmatrix}, \tag{5}$$

where the submatrices A and B take the following general form for hybrid kernels:

$$A_{ia,jb} = \delta_{ij}\delta_{ab}(\varepsilon_a - \varepsilon_i) + \langle aj|\, ib\rangle - \alpha\langle aj|\, bi\rangle + (1-\alpha)\langle a|\frac{\partial V_{XC}}{\partial \rho} j^* b|i\rangle, \tag{6}$$

$$B_{ia,jb} = \langle ab|\, ij\rangle - \alpha\langle ab|\, ji\rangle + (1-\alpha)\langle a|\frac{\partial V_{XC}}{\partial \rho} b^* j|i\rangle, \tag{7}$$

where in expressions (6) and (7) α represents the fraction of the non-local HF exchange in the xc-kernel and ALDA is assumed in the last terms of both equations.

Now, let us consider the diagonal elements of the RPA matrix, which corresponds to the diagonal elements of the matrix A,

$$A_{ia,ia} = (\varepsilon_a - \varepsilon_i) + \langle ai|\, ia\rangle - \alpha\langle ai|\, ai\rangle + (1-\alpha)\langle a|\frac{\partial V_{XC}}{\partial \rho} i^* a|i\rangle. \tag{8}$$

The third element in the right-hand side of expression (8) is responsible for recovering the too high occupied-virtual energy difference obtained in the KS equation when a hybrid xc-functional, containing a fraction of the HF exchange, is used. This simple observation suggests that a possible strategy is to employ the non-local HF exchange of the kernel only for the diagonal elements of the A matrix, while treating at the simpler ALDA level (no HF exchange) all the off-diagonal elements of the A matrix and the full B matrix. With this choice, which we call Hybrid Diagonal Approximation (HDA), the matrices A and B take the following expressions:

$$A_{ia,jb} = \delta_{ij}\delta_{ab}(\varepsilon_a - \varepsilon_i - \Delta_{ia}) + \langle aj|\, ib\rangle + \langle a|\frac{\partial V_{XC}}{\partial \rho} j^* b|i\rangle, \tag{9}$$

$$B_{ia,jb} = \langle ab|\, ij\rangle + \langle a|\frac{\partial V_{XC}}{\partial \rho} b^* j|i\rangle, \tag{10}$$

where in expression (9), we have introduced a diagonal corrective term,

$$\Delta_{ia} = \alpha\langle ai|\, ai\rangle + \alpha\langle a|\frac{\partial V_{XC}}{\partial \rho} i^* a|i\rangle. \tag{11}$$

In expression (11), the second term is much smaller than the first one and can be safely neglected. With the expressions (9) and (10) for the A and B matrix, the difference A-B is still diagonal as it is customary in TDDFT with local kernels, so it is possible to solve the RPA-like equation with respect to Y and obtain again conventional Casida equation (3) for the Ω matrix, with the only difference being limited to the eigenvalue differences, which must be corrected by term (11).

Importantly, following this approach, the number of needed exchange integrals is only (Nocc × Nvirt) instead of $(\text{Nocc} \times \text{Nvirt})^2$, i.e., it is greatly reduced. The implementation of such a scheme starting from a Casida code is straightforward: the elements of the Ω matrix are calculated according to the conventional ALDA expressions with the exception of the diagonal elements, while the orbital energy differences are corrected according to Eqs. (9) and (11). In correction (11), the first term is calculated numerically, while the second term is neglected. Since the Davidson method is usually employed to diagonalize the Ω matrix, only the lowest part of the excitation spectrum is obtained. Therefore, it is not necessary to correct all the diagonal elements of the A matrix, but only those which correspond to excitation energies not too far from the energy range of the spectrum extracted by the Davidson procedure. To this purpose, we have introduced a cutoff parameter that can be chosen in input.

B. Complex polarizability TDDFT formulation

Despite the efficiency of numerical diagonalization techniques such as the Davidson one, it becomes hard to calculate valence

photoabsorption spectra over a wide excitation energy range when large systems are considered. The Davidson iterative algorithm, generally employed in all the TDDFT codes, which use the Casida method, is efficient on large Ω matrices, but is limited to extracting a relatively small number of lowest eigenvalues and eigenvectors. Therefore, the Casida TDDFT algorithm remains efficient for large systems only when attention is focused on few low-energy transitions, but cannot be employed in practice to calculate a photoabsorption spectrum over a wide energy range, often necessary for a thorough simulation of and comparison with an experiment. As the molecule/cluster size increases, the diagonalization problem becomes more and more pathological, eventually rendering the approach unfeasible. In order to overcome this problem, we have recently proposed the complex polarizability TDDFT (polTDDFT) algorithm.[13] This approach is able to treat very large systems and avoid the bottleneck of the diagonalization via a direct solution of the response equations. The reader is referred to the original work for a detailed description of the algorithm,[13] together with its implementation in the ADF program.[14]

In practice, the photoabsorption spectrum $\sigma(\omega)$ is calculated point by point, from the imaginary part of the dynamical polarizability $\alpha(\omega)$,

$$\sigma(\omega) = \frac{4\pi\omega}{c}\,\mathrm{Im}[\alpha(\omega)]. \tag{12}$$

This expression is of practical interest when the polarizability is calculated for complex frequency, i.e., $\omega = \omega_r + i\omega_i$, where the real part ω_r is the scanned photon frequency (energy) and ω_i is the imaginary part, which corresponds to a broadening of the discrete lines and can be interpreted as a pragmatic inclusion of the excited states finite lifetime. The complex dynamical polarizability is calculated by solving the following non-homogeneous linear system:

$$[\mathbf{S} - \mathbf{M}(\omega)]\mathbf{b} = \mathbf{d}. \tag{13}$$

In Eq. (9), **S** is the overlap matrix between fitting functions, **b** is the unknown vector with the expansion coefficients $b_\mu(\omega)$ of $\rho_z^{(1)}$, **d** is the frequency-dependent vector corresponding to the known non-homogeneous term, and finally the elements of the frequency-dependent matrix **M** are

$$M_{\mu\nu} = \langle f_\mu | \chi_{KS}(\omega) K | f_\nu \rangle. \tag{14}$$

In Eq. (14), χ_{KS} refers to the Kohn–Sham frequency-dependent dielectric function and K to the kernel. Notice that the matrix element is between density fitting functions, so the present implementation of the algorithm allows one to employ only density dependent kernels. For this reason, the density matrix dependent HF exchange kernel, which is an ingredient of hybrid functionals, is ruled out. The original characteristic of the polTDDFT method is the introduction of a simple approximation, which enables the construction of $\mathbf{M}(\omega)$ as a linear combination of *frequency independent* matrices $\mathbf{G}^k$ with *frequency-dependent* coefficients $s_k(\omega)$, with the following expression:

$$\mathbf{M}(\omega) = \sum_k s_k(\omega)\mathbf{G}^k. \tag{15}$$

With this idea, a set of matrices $\{\mathbf{G}^k\}$ is calculated and stored only once at the beginning, and then the matrix $\mathbf{M}(\omega)$ is calculated very rapidly at each photon energy ω, as a linear combination of the $\{\mathbf{G}^k\}$ matrices with the following coefficients:

$$s_k(\omega) = \frac{4\bar{E}_k}{\omega^2 - \bar{E}_k^2}, \tag{16}$$

where in expression (16) $\bar{E}_k$ refers to the center of the interval which discretizes the excitation energy variable and in the original formulation, corresponds to the difference between virtual and occupied orbital energies: ε_a-ε_i.

The discrepancies observed between the polTDDFT-HDA and the Casida TDDFT HDA results must be ascribed to the approximations inherent with the polTDDFT algorithm, namely, the choice of the fitting functions to represent the matrix of Eq. (13) and the energy discretization of Eq. (15).

Coming now to the present proposal, in order to apply within the polTDDFT algorithm the HDA approach already discussed for the Casida procedure, it is enough to correct the orbital energy differences with same corrective term (11) as already carried out for expression (9): ε_a-ε_i-Δ_{ia}. With this "rescaling" of the excitation energies, the occupied-virtual pairs will change their position along the excitation energy axis, and expression (16) can be employed to calculate the coefficients $s_k(\omega)$ to build matrix (15) at any given photon energy. Also, in this case, in correction (11), the first term is calculated numerically, while the second term is neglected and a cutoff parameter is introduced in order to avoid corrections of terms so high in energy that do not play a significant role in the calculation.

III. COMPUTATIONAL DETAILS

All the DFT KS calculations reported in this work were performed employing a TZP basis of STO functions (included in the ADF database) and the B3LYP hybrid xc-functional. The TDDFT calculations were carried out after the KS section and were performed with the Casida or the polTDDFT algorithms. For the Casida procedure, both the full B3LYP kernel and the simplified HDA scheme have been employed and compared, whereas the polHDA-B3LYP level is the only available scheme for the hybrid functional within polTDDFT. For both Casida and polTDDFT, the HDA has been implemented by exploiting the parallelization at the general Message Passing Interface (MPI) level. The Casida scheme furnishes the spectra in terms of discrete lines, which have been broadened with Lorentzian functions of HWHM = 0.075 eV in the figures. The polTDDFT furnishes spectra which are already broadened, and in order to be consistent with the Casida broadened profiles, the imaginary part of the photon energy [see ω_i after Eq. (12)] has been set to 0.075 eV as well. When comparing with experimental data, we employed a broadening equal to the experimental resolution (HWHM = 0.5 eV). All the calculations were performed with a local version of the ADF code, while the HDA implementation for both Casida and polTDDFT algorithms will be distributed in a forthcoming ADF release. The calculations for the gold cluster in Sec. IV C were performed employing the Zero Order Regular Approximation (ZORA) in order to include relativistic effects at the scalar level.

IV. RESULTS AND DISCUSSION

We have fully tested the performances of the HDA scheme implemented in this work on two small systems (NH_3, C_6H_6) and

a medium-sized ligand-protected metal cluster $Au_{25}(SR)_{18}$. The goal is to achieve a firm assessment of the accuracy of the HDA at both Casida and complex polarization algorithms using the hybrid B3LYP functional with respect to the full B3LYP kernel at the Casida level as well as to the experiment. For the metal cluster, also an analysis of the performances in terms of computational saving will be provided. Moreover, we have also tested the HDA with respect to the full kernel only at the Casida level for an additional set of seven systems, in order to show the effect of HDA on the excitation energies and the oscillator strengths, to corroborate the HDA validity and provide at least an estimate of the expected errors.

At the moment, the program is installed on a HP ProLiant DL580 Gen10 server (with four processors each with 18 cores Intel® Xeon® Gold 6140 CPU @ 2.30 GHz, in total, 72 cores and 728 GB of RAM), on which the present calculations were run using 24 cores at most. The implementation is general MPI.

A. NH_3

In the upper panel of Fig. 1, we have reported three calculated spectra for NH_3: (1) the Casida profile at the B3LYP level with the full kernel (blue line), (2) the Casida profile at the B3LYP level with the HDA kernel (red line), and (3) the polTDDFT profile at the B3LYP level with the HDA kernel (green line), which we call hereafter pol-HDA. To validate the HDA approach, we compare the Casida full kernel with respect to HDA. As apparent from Fig. 1, the two profiles are almost superimposed: a very modest discrepancy is seen for the feature around 13.6 eV, but the difference is modest, the energy difference in peak positions is below 0.1 eV, and the intensity is also only slightly affected. This observation demonstrates the accuracy of the HDA scheme. It is worth noting that if a pure ALDA kernel would have been chosen in the TDDFT procedure after a B3LYP KS calculation, the first peak around 6 eV would have been shifted by about 0.7 eV to higher energy. This demonstrates our working hypothesis that the role of the non-local HF exchange in the kernel is limited to the diagonal elements, providing a robust argument to justify the HDA scheme. Also, the pol-HDA profile is in excellent agreement with the Casida HDA one, suggesting that the approximations introduced by polTDDFT are adequate for a proper description of the excitation process.

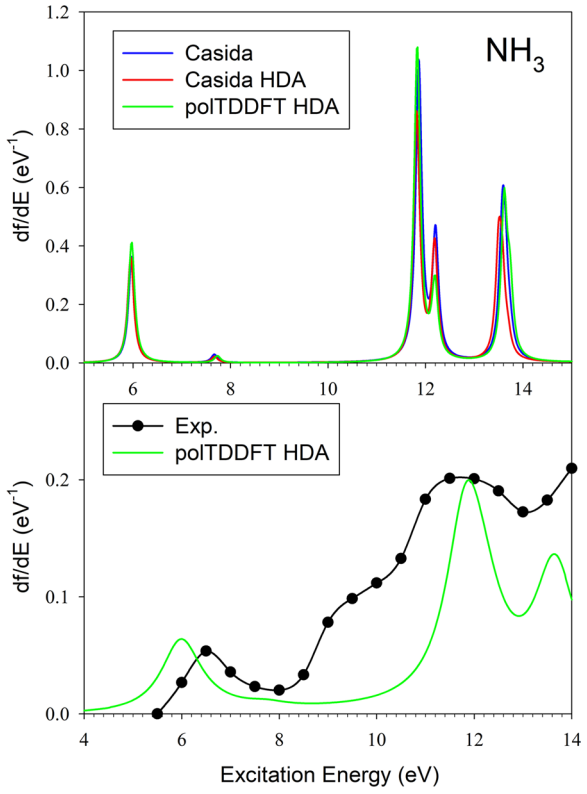

FIG. 1. Valence excitation spectra of NH_3. Upper panel: calculated profile with the Casida approach (blue line), Casida HDA (red line), and polTDDFT (green line), broadened with HWHM = 0.075 eV. Lower panel: low-resolution experimental data[31] (black line and circles) and calculated profile with polTDDFT (green line), broadened with HWHM = 0.5 eV.

Although the goal of the present work is to assess the validity of the HDA with respect to the full kernel for B3LYP, it is also interesting to compare the theoretical excitation spectrum with respect to the experiment, to have an indication of the adequacy of the B3LYP xc-functional to describe valence excitation spectra. For this reason, the low-resolution total photoabsorption experimental measurement from the work of Brion *et al.*[31] has been shown (black line) in the lower box of Fig. 1, where in the reported calculated profile, the same broadening as the experimental resolution has been employed (HWHM = 0.5 eV). Note that we have preferred to employ a much lower broadening (HWHM = 0.075 eV) for comparison among different computational schemes (upper panel) to amplify possible differences.

The first band with a maximum at 6.5 eV is assigned by present calculations to the $3a_1$ (HOMO) → $4a_1$ (mixed valence –Rydberg 3s), in line with previous assignments. The energy position is properly described by theory, with few tenths of eV of error if we take the vertical values, and the absolute intensity is in fairly good agreement with the experiment as well. The next experimental feature is a very weak vibrational progression (visible in the high-resolution experiment reported in Ref. 31) encompassing the region between 7.5 eV and 8.5 eV, which is properly described by theory as a very weak peak; also, in this case, the transition corresponds to the excitation of the HOMO $3a_1$ to the 2e virtual orbital, with mixed valence, Rydberg nature, but this time of 3p instead of 3s nature. From 8.8 eV up to 11 eV, at least four different vibrational progressions have been identified in the experimental data,[31] which are not present in the calculated profiles. This is not surprising since these correspond to high Rydberg states *n*s with n > 3, which are not supported by the present theoretical approach for two reasons: (1) the B3LYP xc-functional does not have the correct asymptotic Coulomb behavior and, therefore, cannot support high-lying Rydberg states; (2) even using xc-functionals with the correct asymptotic behavior, for example Long-range Corrected (LC) ones[32] or more simple models such as LB94[33] or SAOP,[34] the description of high-lying Rydberg states requires improved basis set, augmented with very diffuse functions. Since the present HDA scheme has been proposed in order to save computational efforts when B3LYP is used in TDDFT calculations of large systems where Rydberg state does not play a relevant role, we did not try to improve the description of this spectral region. The ionization limit of NH_3 is around

10.85 eV;[31] therefore, beyond this energy, the comparison with the experiment should include photoionization channels which are not considered in the present TDDFT formalism. Anyway, the "shape resonance" around 12 eV is properly described by two discrete bands in the calculated spectrum, and also, the following intensity increase around 14 eV is consistent with the discrete transition calculated at 13.7 eV. Therefore, we can conclude the analysis of NH_3 saying that B3LYP is adequate for a quantitative description of the valence excitation spectrum, with errors of few tenths of eV, and that HDA and polHDA exhibit similar accuracy as the full kernel simulations. Known limitations regarding Rydberg states are not expected to be important for applications to large systems. In any case, the possibility to use LC functionals and the basis set supplemented by diffuse functions is possible also in connection with the HDA approach, so this limitation is not intrinsic to the methodology.

B. C_6H_6

The same analysis pursued for NH_3 has been applied to C_6H_6, and the results are shown in Fig. 2: in the upper panel, the three calculated profiles broadened with HWHM = 0.075 eV are reported, while in the lower panel, the polTDDFT calculation broadened with the experimental resolution corresponding to an HWHM of 0.5 eV is reported together with the low-resolution total photoabsorption experimental data from Feng *et al.*[35] (black line). This time, the results of the Casida scheme using the HDA are in good agreement with the full kernel results, with differences in excitation energies below 0.3 eV in the worst cases. Intensities are properly reproduced as well, with modest discrepancies, the largest being an underestimate of 30% of the transition at 9.7 eV, but notice that the intensity of first strong π–π^* transition at 7 eV is underestimated by only 5%. When the pol-HDA is considered, some discrepancies are apparent above 11 eV, but limited to the intensity of the transitions, whereas their energy positions remain in excellent agreement with the Casida results. Anyway, these discrepancies are inherent to the polTDDFT scheme and not to the HDA approach.

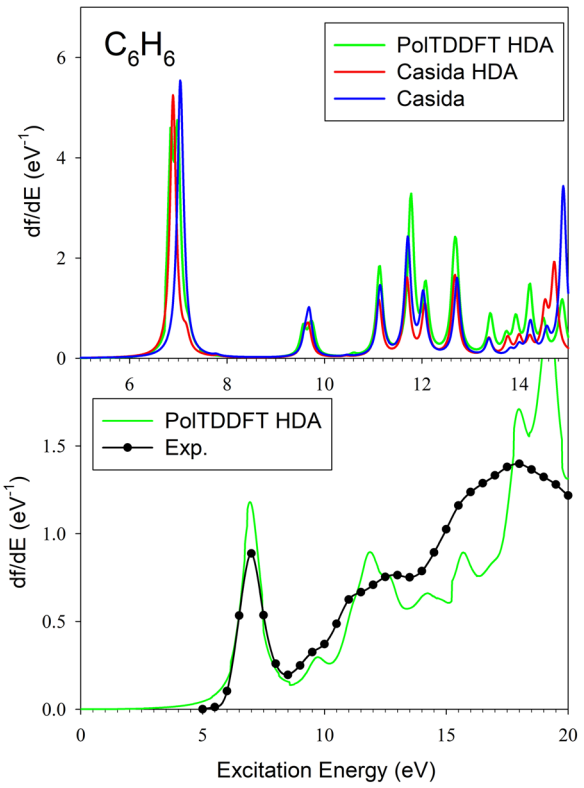

FIG. 2. Valence excitation spectra of C_6H_6. Upper panel: calculated profile with the Casida approach (blue line), Casida HDA (red line), and polTDDFT (green line), broadened with HWHM = 0.075 eV. Lower panel: low-resolution experimental data[35] (black line and circles) and calculated profile with polTDDFT (green line), broadened with HWHM = 0.5 eV.

Also, for C_6H_6, it is interesting to compare the calculated results with respect to low-resolution measurement, in order to assess the quality of the B3LYP xc-functional. The first intense experimental band with a maximum at 6.94 eV has been ascribed[35] to the valence π–π^* transition $^1E_{1u} \leftarrow {}^1A_{1g}$, confirmed by present calculations at 6.89 eV in excellent quantitative agreement. Also, the absolute normalization of the first peak is satisfactory, considering the arbitrariness of the broadening and the irregular shape of the experimental band.

For C_6H_6, the first vertical ionization energy falls at 9.45 eV, and the tiny structures in the range 8–9.5 eV have been ascribed to vibrational progressions of Rydberg transitions,[35] not supported by the present formalism. Beyond the first ionization limit, the photoionization continuum should be included for comparison with the experiment; however, the simple discrete spectrum here calculated is nevertheless able to describe with semi-quantitative accuracy the weak spectral features measured above 9.45 eV. In summary, also for C_6H_6, the HDA approximation is proven to be accurate, and B3LYP is confirmed to be able to describe properly the valence excitation spectrum, with quantitative agreement for the first π–π^* transition.

C. $[Au_{25}(SCH_3)_{18}]^-$

Finally, we tested the performance of the HDA approach on a much more complex system, in particular, on a medium-sized gold cluster protected by thiolate ligands. We choose the $[Au_{25}(SCH_3)_{18}]^-$ system for several reasons: first, the structure of this system has been completely characterized by x-ray diffraction;[36] second, experimental photoabsorption data are available for comparison;[37] and third, this system has been already employed in our previous work to validate and assess the performances of computational protocols[38] such as xc-functional and basis set choice, ligand simplification, and geometry optimization protocols for ligands.

In Fig. 3, we report the results of the Casida full kernel and HDA, as well as the pol-HDA calculated profiles, together with experimental data.[37] Note that in this case, we did not consider absolute intensity, so we adopt an arbitrary unit intensity scale. Note also that the calculations have been performed for SR ligands with R = CH_3, to allow us to perform full kernel B3LYP TDDDFT calculations with our computational resources, while the experiment has been performed with SR′ ligands with R′ = $CH_2CH_2C_6H_5$ (this simplification will be further discussed below). Figure 3 shows an

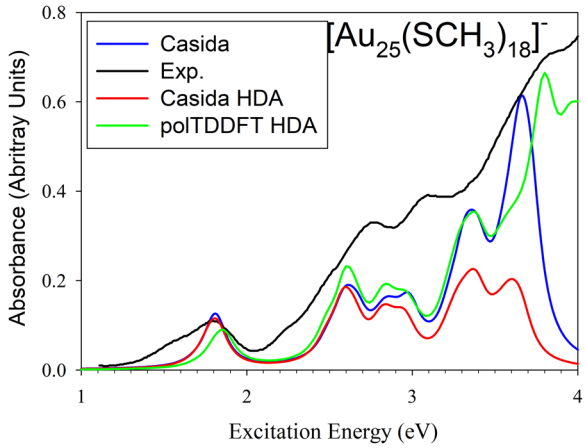

FIG. 3. Valence excitation spectra of $[Au_{25}(SCH_3)_{18}]^-$. Calculated profile with the Casida approach (blue line), Casida HDA (red line), and polTDDFT (green line), broadened with HWHM = 0.075 eV and experimental data[37] (black line).

excellent match between full kernel and HDA TDDDFT Casida profiles apart from a minor deviation around 3.4 eV. Regarding the pol-HDA profile, it follows very well the Casida ones up to 2.6 eV, with a minor deterioration (less than 0.1 eV) for the first peak at 1.8 eV. Beyond 2.6 eV, the polTDDFT-HDA is in better agreement with the full kernel Casida than with the HDA one. The comparison with respect to the experiment is fairly good: for the first peak at 1.8 eV, the agreement between the Casida results and the experiment is quantitative, with pol-HDA worsening the agreement by less than 0.1 eV. We can recall that this first peak is quite hard to be properly reproduced, despite the previous studies[38] improving the basis set, changing the xc-functional, including full ligands (not simplified methyl residues) in the calculation, and fully or partially optimizing the geometry. At the moment, the B3LYP seems to be the best xc-functional to reproduce quantitatively the experimental data. Additional spectral features appear in the experiment at higher energies, namely, at 2.75 eV, 3.1 eV, and 3.9 eV, and all of them are properly reproduced by theory, with deviations of few tenths of eV. It must be considered that, in the region around 3 eV, the nature of the ligand is important to properly assess the spectrum, so the simplification of $R' = CH_2CH_2C_6H_5$ with the smaller $R = CH_3$ can be the cause of this deterioration. In fact, it has been shown that, at the SAOP-TZP level, the substitution of R′ with R induces an energy widening between the two peaks at 2.47 eV and 3.0 eV, see Fig. 3 and Table I in Ref. 38.

Finally, it is worth mentioning the CPU time of the calculations on this cluster. The calculations ran on the hardware described in the computational details, employing 24 cores for each run. In terms of elapsed time, the Casida with a full kernel spent 60.6 h, Casida with an HDA 8.75 h, and polTDDFT 16.4 h. The HDA allows us to get a factor of seven in the speedup of Casida procedure, and polTDDFT is four times faster than Casida with full kernel but allows one to calculate the spectrum to much higher energies.

D. Specific tests with the Casida method

In order to assess the effect of the HDA approximation, we decided to compare the B3LYP full kernel results with respect to the HDA at the Casida level for a set of seven additional molecules. In order to span different chemical situations, we considered five paradigmatic organic molecules (taken from Refs. 39 and 40): all-E-hexatriene (C_6H_8), pyridine (C_5H_5N), cytosine, 6,6′-difluoro-indigo, *p*-benzoquinone ($C_6H_4O_2$), together with a metallorganic complex ferrocene $Fe(C_5H_5)_2$, and finally a chiral model metal cluster, Ag_8.[15,41] In Figs. 4–6, we have reported the calculated

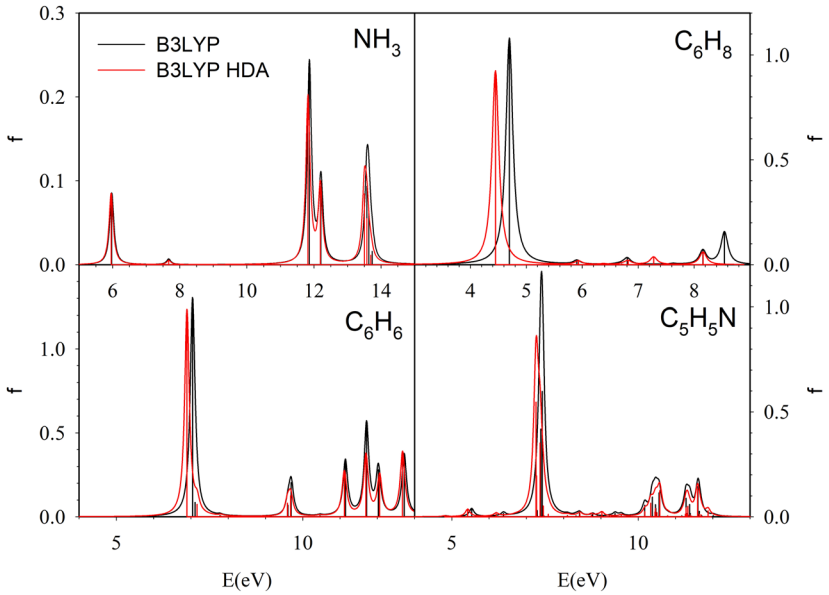

FIG. 4. Valence excitation spectra of NH_3, C_6H_8 (all-E-Hexatriene), C_6H_6, and C_5H_5N (pyridine). Calculated profiles with the Casida full kernel approach (black lines) and Casida HDA (red lines); discrete excitations are reported, together with broadened Lorentzian profiles by HWHM = 0.075 eV.

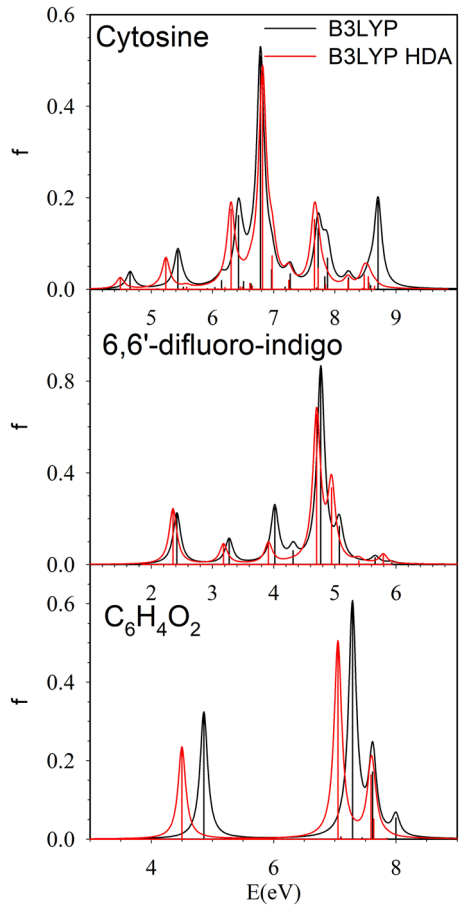

FIG. 5. Valence excitation spectra of cytosine, 6,6′-difluoro-indigo, and $C_6H_4O_2$ (*p*-benzoquinone). Calculated profiles with the Casida full kernel approach (black lines) and Casida HDA (red lines); discrete excitations are reported, together with broadened Lorentzian profiles by HWHM = 0.075 eV.

spectra both as discrete lines and as broadened profiles with Lorentzian functions of HWHM = 0.075 eV by using black lines for the full kernel and red lines for HDA. Since we add discrete lines in the chiro-optical spectra, in our analysis, we included also the three systems considered in Secs. IV A–IV C in order to see the HDA effects on the individual discrete lines of these systems as well.

In Fig. 4, NH_3 together three small organic molecules (C_6H_6, C_6H_8, and C_5H_5N) is considered: as a general statement, the difference between the calculated spectra are modest, although one should consider that different energy scales have been employed in the figures since the spectra are quite different from each other. Only for benzene and pyridine, we have employed the same energy scale due to their chemical similarity. In general, the errors in excitation energies are of the order of few tenths of eV, not exceeding 0.3 eV. All-E-hexatriene (C_6H_8) gives the worst agreement; in this case, the spectrum is dominated by only one transition around 4.7 eV. It is important to underline that we do not advocate employing HDA for small systems like the present ones, for which superior methods are available and practicable. We consider here small systems simply to assess HDA performance and have an idea of its accuracy when it is applied to large systems, where the B3LYP TDDFT full kernel scheme would be not practicable at all.

In Fig. 5, larger organic molecules are considered. Apart from *p*-benzoquinone, whose spectra appear much more complex and richer of spectral features, also in this case, all the spectra calculated at the HDA level show only modest differences with respect to the full kernel results, and in general, the excitation energy discrepancies remain below 0.2 eV. In occasional circumstances, more pronounced deterioration is apparent, such as, for example, the feature around 4 eV in 6,6′-difluoro-indigo and the first strong peak of *p*-benzoquinone, the latter corresponding to the largest found disagreement in present study which is 0.4 eV. In general, the HDA performs better when the molecule is larger and the spectrum is rich of features, and this is probably due to the fact that when many transitions are close together in a narrow energy interval, their mutual coupling tends to reduce the effect of the non-local xc-kernel. Such an effect is particularly evident from Fig. 6, where the largest systems are compared with each other.

We start the discussion of Fig. 6 noting that the discrete excitation spectrum of the $[Au_{25}(SCH_3)_{18}]^-$ cluster is characterized by groups of discrete excitation, well separated by gaps, for example, there is a large gap between 1.8 eV and 2.4 eV and two narrow ones between 2.6 eV and 2.8 eV and between 3.0 eV and 3.2 eV. The HDA simulates nicely such feature of the excitation energies, but also the intensity distributions is very well reproduced, as demonstrated by the mutual agreement of the broadened profiles as well. The only appreciable yet modest deterioration is around 3.3 eV, where HDA slightly underestimates the intensity.

For $Fe(C_5H_5)_2$, the spectrum is dominated by the intense transition at 6.9 eV, which is shifted by only 0.1 eV and slightly reduced in intensity when HDA is employed. The remaining spectral features are less prominent and are satisfactorily reproduced by HDA.

Finally, we have included in the present analysis the bare cluster Ag_8, which was already employed previously as a model system to study the Circular Dichroism (CD) in chiral metal clusters.[15,41] Also, in this case, the photoabsorption oscillator strengths (left lower panel of Fig. 6) calculated by HDA are in good agreement with the full kernel B3LYP results, and the first strong transition at 1.3 eV is underestimated by only 0.1 eV and slightly reduced in intensity when HDA is introduced. In the right lower panel of Fig. 6, the Ag_8 CD expressed as Rotatory strength (R) is reported. It is worth noting that the HDA is suitable to reproduce quantitatively the peak positions, their sign, and also the R values. For the HDA scheme, the usual gauge-dependence of the CD spectrum is expected, so the employment of a good quality basis set is necessary. The present basis set of TZP size has proven to be suitable in a previous study.[15]

We conclude from this section that the HDA scheme has proven suitable to reproduce nicely the photoabsorption and CD spectra of molecular systems, ranging from small organic molecules to metallorganic complexes and large metal clusters.

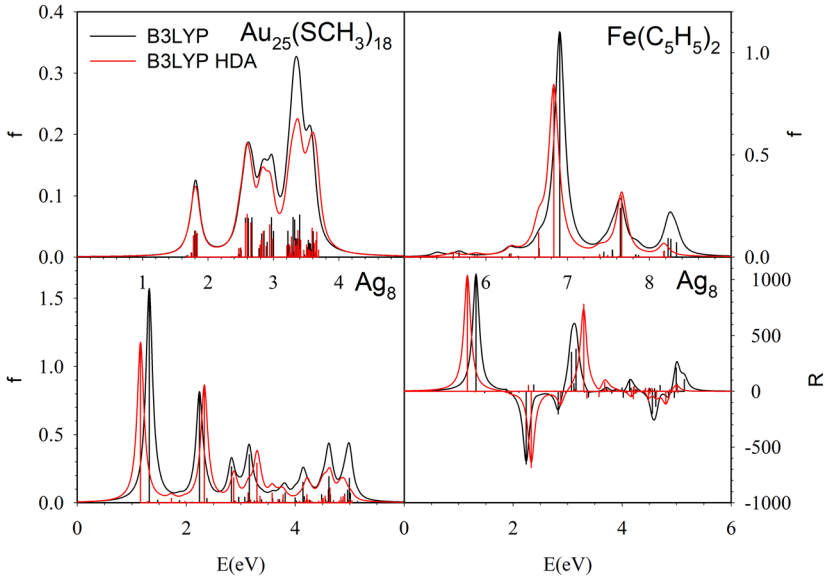

FIG. 6. Valence excitation spectra of $[Au_{25}(SCH_3)_{18}]^-$, $Fe(C_5H_5)_2$, and Ag_8. Calculated profiles with the Casida full kernel approach (black lines) and Casida HDA (red lines); discrete excitations are reported, together with broadened Lorentzian profiles by HWHM = 0.075 eV. For Ag_8, also the Rotatory strengths (R) are reported (right lower panel) in units of 10^{-40} esu^2 cm^2.

V. CONCLUSIONS

We propose and develop an approximate but physically grounded and accurate approach to greatly accelerate TDDFT simulations using hybrid xc-functionals, which we name Hybrid Diagonal Approximation (HDA). It is known that when hybrid xc-functionals are employed to solve the TDDFT equations, the kernel is called to recover the too wide energy gap introduced in the occupied-virtual orbital energy differences by the HF exchange. In this work, we show that this correction is essentially given by the diagonal part of the kernel, thus justifying the present simplified HDA scheme, in which the fraction of the HF exchange is employed only for the diagonal matrix elements, while for off-diagonal matrix elements, the simple ALDA is assumed. HDA is especially convenient in connection with Slater Type Orbitals (STO) basis sets as in the present work. In fact, the current TDDFT codes using STO basis sets are not efficient because the non-local HF exchange contribution of the kernel needs a CPU-demanding density fitting procedure to calculate two-electron integrals. Additionally, although the Gaussian Type Orbital (GTO) basis set does not suffer this problem due to its analytical product expansions,[28,29] significant speedups by a factor larger than four have still been achieved in explorative tests using GTO and the NWChem suite of codes.[42] In fact, HDA is a general approach and, therefore, can also help accelerate hybrid calculations on large molecules that use density fitting techniques for GTOs since density fitting for the exchange terms is known to be problematic for large basis sets. Moreover, the implementation of HDA is rather straightforward since it consists in disabling the calculation of the non-local kernel for the extradiagonal elements of the omega matrix rescaling the ALDA contribution to 100%, a procedure which should be easily implementable in any TDDFT code.

We applied the HDA approach to ten different systems, conducting a full comparison with experiment in particular for NH_3, C_6H_6, and $[Au_{25}(SCH_3)_{18}]^-$ as test cases, finding excellent agreement with respect to both the full kernel and experimental data. For the metal cluster, a speedup of a factor of 7 has been obtained with respect to the full kernel implementation. The TDDFT-HDA/B3LYP protocol, therefore, promises to greatly facilitate achieving a quantitative description of the optical properties of medium-sized and complex systems, thanks to its computational efficiency, especially in the field of nanoclusters. Here, we have also developed and tested the implementation of the HDA within the complex polarization algorithm (polTDDFT) and proved that the approach is equally accurate and efficient, while allowing for the prediction of the high-energy part of the spectrum.

In addition to the three systems which we have analyzed in detail, we have also tested the validity of the HDA within the Casida approach by comparison with full kernel results for seven additional systems, ranging from simple to larger organic molecules, one metallorganic complex, and one chiral bare metal cluster. In all cases, the HDA has proven to be a good approximation of the full kernel results, with deviations with respect to excitation energies usually well below 0.3 eV and a slight reduction in the calculated intensity. For the metal cluster, the HDA has given an excellent quantitative reproduction of the CD spectrum.

As an overall conclusion of this work, we believe that the HDA is very promising to extend the range of applicability of TDDFT/B3LYP and in general, TDDFT using hybrid functionals, to very large systems, when the non-local Fock exchange kernel becomes prohibitive, a problem that plagues primarily non-GTO basis set, such as STO and plane waves (PWs), and also GTO basis sets.

Future extensions of the present methodology will include xc-functionals with Long-range Correction (LC), which should improve the description of virtual orbitals or with Short-range Correction (SC), for example, for applications in core excitation spectra,[24] as well as the implementation in codes using GTO and plane wave basis sets.

ACKNOWLEDGMENTS

The authors are grateful to Edoardo Aprà for fruitful discussions and explorative tests using the NWChem suite of codes. A.F. acknowledges stimulating discussions with Nicola Durante. MS is grateful to Erik van Lenthe and Stan van Gisbergen of SCM (Amsterdam) for fruitful discussions and technical assistance during the implementation within the ADF program. Computational support from the CINECA supercomputing center within the ISCRA program is gratefully acknowledged. The authors are grateful to the Stiftung Beneficentia for a generous grant employed to set up a computational server. Support from Trieste University within the FRA program is gratefully acknowledged.

DATA AVAILABILITY

The data that support the findings of this study are available from the corresponding author upon reasonable request.

REFERENCES

[1] V. Barone, WIREs Comput. Mol. Sci. **6**, 86 (2016).
[2] M. E. Casida, *Recent Advances in Density-Functional Methods*, edited by D. P. Chong (World Scientific, Singapore, 1995), p. 155.
[3] A. Görling, H. H. Heinze, S. Ph. Ruzankin, M. Staufer, and N. Rösch, J. Chem. Phys. **110**, 2785 (1999).
[4] K. Yabana and G. F. Bertsch, Phys. Rev. B **54**, 4484 (1996).
[5] M. A. L. Marques, A. Castro, G. F. Bertsch, and A. Rubio, Comput. Phys. Commun. **151**, 60 (2003).
[6] B. Walker, A. M. Saitta, R. Gebauer, and S. Baroni, Phys. Rev. Lett. **96**, 113001 (2006).
[7] S. Grimme, J. Chem. Phys. **138**, 244104 (2013).
[8] C. Bannwarth and S. Grimme, Comput. Theoret. Chem. **1040-1041**, 45 (2014).
[9] T. J. Zuehlsdorff, N. D. M. Hine, J. S. Spencer, N. M. Harrison, D. J. Riley, and P. D. Haynes, Chem. Phys. **139**, 064104 (2013).
[10] S. Malola, L. Lehtovaara, J. Enkovaara, and H. Häkkinen, ACS Nano **7**, 10263 (2013).
[11] M. Noda, K. Ishimura, K. Nobusada, K. Yabana, and T. Boku, J. Comput. Phys. **265**, 145 (2014).
[12] K. Iida, M. Noda, K. Ishimura, and K. Nobusada, Phys. Chem. A **118**, 11317 (2014).
[13] O. Baseggio, G. Fronzoni, and M. Stener, J. Chem. Phys. **143**, 024106 (2015).
[14] O. Baseggio, M. De Vetta, G. Fronzoni, M. Stener, and A. Fortunelli, Int. J. Quantum Chem. **116**, 1603 (2016).
[15] O. Baseggio, D. Toffoli, G. Fronzoni, M. Stener, L. Sementa, and A. Fortunelli, J. Phys. Chem. C **120**, 24335 (2016).
[16] O. Baseggio, M. De Vetta, G. Fronzoni, M. Stener, L. Sementa, A. Fortunelli, and A. Calzolari, J. Phys. Chem. C **120**, 12773 (2016).
[17] A. D. Becke, J. Chem. Phys. **140**, 18A301 (2014).
[18] N. Mardirossian and M. Head-Gordon, Mol. Phys. **115**, 2315 (2017).
[19] A. D. Becke, J.Chem.Phys. **98**, 5648 (1993).
[20] P. J. Stephens, F. J. Devlin, C. F. Chabalowski, and M. J. Frisch, Phys. Chem. **98**, 11623 (1994).
[21] A. Baiardi, M. Mendolicchio, V. Barone, G. Fronzoni, G. A. Cardenas Jimenez, M. Stener, C. Grazioli, M. de Simone, and M. Coreno, J. Chem. Phys. **143**, 204102 (2015).
[22] M. Mendolicchio, A. Baiardi, G. Fronzoni, M. Stener, C. Grazioli, M. de Simone, and V. Barone, J. Chem. Phys. **151**, 124105 (2019).
[23] A. Savin, in *Recent Developments and Applications of Modern Density Functional Theory*, edited by J. M. Seminario (Elsevier, Amsterdam, 1996), p. 327.
[24] N. A. Besley, M. J. G. Peach, and D. J. Tozer, Phys. Chem. Chem. Phys. **11**, 10350 (2009).
[25] E. J. Baerends, D. E. Ellis, and P. Ros, Chem. Phys. **2**, 41 (1973).
[26] C. Fonseca Guerra, J. G. Snijders, G. te Velde, and E. J. Baerends, Theor. Chem. Acc. **99**, 391 (1998).
[27] S. J. A. van Gisbergen, J. G. Snijders, and E. J. Baerends, Comput. Phys. Commun. **118**, 119 (1999).
[28] A. Fortunelli and O. Salvetti, J. Comput. Chem. **12**, 36 (1991).
[29] A. Fortunelli and O. Salvetti, Chem. Phys. Lett. **186**, 372 (1991).
[30] E. K. U. Gross and W. Kohn, Adv. Quantum Chem. **21**, 255 (1990).
[31] G. R. Burton, W. F. Chan, G. Cooper, and C. E. Brion, Chem. Phys. **177**, 217 (1993).
[32] H. Iikura, T. Tsuneda, T. Yanai, and K. Hirao, J. Chem. Phys. **115**, 3540 (2001).
[33] R. van Leeuwen and E. J. Baerends, Phys. Rev. A **49**, 2421 (1994).
[34] O. V. Gritsenko, P. R. T. Schipper, and E. J. Baerends, Chem. Phys. Lett. **302**, 199 (1999).
[35] R. Feng, G. Cooper, and C. E. Brion, J. Electr. Spectrosc., Relat. Phenom. **123**, 199 (2002).
[36] M. W. Heaven, A. Dass, P. S. White, K. M. Holt, and R. W. Murray, J. Am. Chem. Soc. **130**, 3754 (2008).
[37] M. Zhu, C. M. Aikens, F. J. Hollander, G. C. Schatz, and R. Jin, J. Am. Chem. Soc. **130**, 5883 (2008).
[38] O. Baseggio, M. De Vetta, G. Fronzoni, D. Toffoli, M. Stener, L. Sementa, and A. Fortunelli, Int. J. Quantum Chem. **118**, e25769 (2018).
[39] L. Goerigk, J. Moellmann, and S. Grimme, Phys.Chem. Chem. Phys. **11**, 4611 (2009).
[40] M. Schreiber, M. R. Silva-Junior, S. P. A. Sauer, and W. Thiel, J. Chem. Phys. **128**, 134110 (2008).
[41] N. V. Karimova and C. M. Aikens, J. Phys. Chem. A **119**, 8163 (2015).
[42] M. Valiev, E. J. Bylaska, N. Govind, K. Kowalski, T. P. Straatsma, H. J. J. van Dam, D. Wang, J. Nieplocha, E. Apra, T. L. Windus, and W. A. de Jong, Comput. Phys. Commun. **181**, 1477 (2010).